Cold Regions Science and Technology 97 (2014) 97–103

Contents lists available at ScienceDirect

Cold Regions Science and Technology

journal homepage: www.elsevier.com/locate/coldregions

Measurements of snow slab displacement in Extended Column Tests and comparison with Propagation Saw Tests

A. van Herwijnen [a,*], K.W. Birkeland [b]

[a] WSL Institute for Snow and Avalanche Research SLF, Davos, Switzerland
[b] USDA Forest Service National Avalanche Center, Bozeman, MT, USA

ARTICLE INFO

Article history:
Received 7 December 2012
Received in revised form 5 July 2013
Accepted 8 July 2013

Keywords:
Snow fracture
Snow stability tests
Avalanche forecasting
Particle tracking

ABSTRACT

The Extended Column Test (ECT) has become increasingly popular for assessing snowpack stability. What happens to the snow slab and the underlying weak layer during the test remains largely unknown. Such work has been done for the Propagation Saw Test (PST), but not for the ECT. We therefore analyzed high-speed videos of ECTs and adjacent PSTs using particle tracking to better understand the mechanics of the ECT. Our results show that in an ECT, tapping on one end of the column had no observable effect on the opposite end, and that fracture initiates in an area of the weak layer directly under the shovel at the free edge of the column. We observed no signs of progressive damage accumulation in the weak layer during tapping, but rather a single rapid collapse when fracture initiated. In contrast, in PSTs, we observed slab bending prior to weak layer fracture. During fracture, weak layers in ECTs compact on the order of several mm, similar to measurements obtained from PSTs. Measured propagation speeds, on the order of 20 to 30 m s^{-1}, were also similar to those from PSTs. The similarities between ECT results and those with PSTs give us confidence that the fracture mechanics are similar regardless of the triggering mechanism. From a practical perspective, our results suggest that the ECT is indeed measuring the propensity of a crack to propagate at the small scale of the ECT block, thus providing information on a critically important property of snow stability in our tests.

1. Introduction

Dry snow slab avalanches are preceded by fracture of a weak snowpack layer below a cohesive slab of snow. An initial weak layer crack must first reach a critical size before it expands rapidly, releasing a slab avalanche (e.g. Schweizer et al., 2003). Weak layer cracks can form naturally (e.g., due to snow loading) or artificially (e.g., due to skier loading or explosive triggers). Avalanche workers and researchers utilize snow stability tests to characterize snow stratigraphy and estimate whether a particular slope is stable or unstable. Ideally, results from these tests should provide unambiguous information on the ease of crack initiation and the propensity for crack propagation, both of which are required for snow slab avalanche release (e.g. van Herwijnen and Jamieson, 2007b). However, given the inherent limitations of the various tests in replicating the avalanche release process and the spatially variable nature of the mountain snowpack, snow stability test results are not unambiguous and require expert interpretation (Schweizer and Jamieson, 2010). Nevertheless, a number of different studies demonstrate the usefulness of snow stability tests for assessing avalanche risk (e.g. Föhn, 1987; Simenhois and Birkeland, 2009; van Herwijnen and Jamieson, 2007a).

Snow stability tests consist of isolating a block of snow of pre-defined dimensions and incrementally loading the block up to a maximum load. While one goal of these tests is to identify potential weak layers, the primary goal is to evaluate the load required to fracture them, i.e. to create an initial crack that will propagate. Traditionally, the most commonly used tests were the Rutschblock test (Föhn, 1987), consisting of a 1.5 by 2 m block of snow loaded by a skier, and the compression test, consisting of a 30 by 30 cm block of snow loaded by tapping on a snow shovel (Jamieson, 1999). While the loading step at weak layer fracture mainly relates to crack initiation, additional information on crack propagation is obtained through qualitative fracture observations (e.g. Schweizer and Jamieson, 2010). In recent years, researchers developed two new field tests to investigate fracture initiation and fracture propagation along the weak layer, namely the Extended Column Test (ECT) and the Propagation Saw Test (PST) (Gauthier and Jamieson, 2006, 2008; Sigrist and Schweizer, 2007; Simenhois and Birkeland, 2009; van Herwijnen and Jamieson, 2005).

The ECT involves isolating a block 90 cm cross-slope by 30 cm upslope and then progressively loading one side of the block by tapping on a snow shovel, similar to a compression test (Simenhois and Birkeland, 2006, 2009). Avalanche workers have rapidly adopted the ECT since its introduction in 2006. It has become the most popular stability test in the past two years by SnowPilot users (Chabot et al., 2004), being conducted in almost 80% of the pits (Birkeland and Chabot, 2012). The usefulness of the test as a forecasting tool for predicting avalanche conditions has been studied in several different snow climates and countries (e.g. Ross and Jamieson, 2008; Simenhois and Birkeland,

* Corresponding author. Tel.: +41 814170161.
E-mail address: vanherwijnen@slf.ch (A. van Herwijnen).

0165-232X/$ – see front matter © 2013 Elsevier B.V. All rights reserved.
http://dx.doi.org/10.1016/j.coldregions.2013.07.002

Table 1
Overview of the snow properties at each field site.

Site	N_{ECT}	N_{PST}	θ (degrees)	F	H (m)	ρ_{slab} (kg m^{-3})
A	5	2	0.35	DH	39	194
B	2	2	0.25	SH	37	190
C	1	2	0.36	FC	53	316
D	5	1	0.30	SH	43	143
E	2	2	0.24	SH	67	180
F	3	1	0.22	SH	35	169
G	2	1	0.10	SH	32	248

The number of ECTs (N_{ECT}), the number of and PSTs (N_{PST}), slope angle (θ), weak layer grain form (F), slab depth (H) and mean slab density (ρ_{slab}) are shown for each site. The observed weak layer grain forms were: depth hoar (DH), surface hoar (SH) and faceted grains (FC).

2009; Winkler and Schweizer, 2009). However, the processes leading to weak layer fracture in the ECT have thus far not been investigated.

The PST involves isolating a block that is 30 cm cross-slope by 100 cm upslope (or the weak layer depth, whichever is greater) and then cutting the weak layer with a snow saw until weak layer fracture (Gauthier and Jamieson, 2008). The popularity of the PST has risen steadily since its introduction. It was the third most common field test amongst SnowPilot users for the winter of 2011/12 (Birkeland and Chabot, 2012). In contrast to the ECT, the PST has been the subject of several detailed studies focusing on the mechanics of the test to better understand some of the fundamental processes involved in snow fracture (e.g. Bair et al., 2012; van Herwijnen and Heierli, 2009; van Herwijnen et al., 2010). Much of this work utilizes particle tracking, where a video recording of the test is made with a high speed camera and markers are inserted into the snowpack to analyze snow displacement using particle tracking software.

In this study we apply the same particle tracking technique used in PST studies to the ECT. The goal is to better understand the mechanics of the ECT, such as whether or not the whole block is affected by the tapping, where the fracture initiates, and whether fracture speeds in the ECT are similar to those measured with the PST. An improved mechanical understanding of the test will help to better interpret test results and evaluate potential limitations.

2. Methods

2.1. Data collection

We collected data at seven sites during the 2011/12 winter in southwest Montana, USA (Table 1). At each field site, we did a manual snow profile to obtain information on snow stratigraphy and performed one or several ECTs and PSTs according to the procedure outlined in Greene et al. (2010). In some cases, our ECTs had wider columns, allowing us to better evaluate weak layer fracture at distances farther from the tapping area (Fig. 1a). Our PSTs also had longer columns, and we modified the columns to have slope normal, rather than vertical, column ends, as suggested by other research (Bair et al., 2012; Heierli, 2008; van Herwijnen and Heierli, 2010). After excavating test columns from the surrounding snow cover, we inserted black plastic markers into the snow wall above the weak layer. Using a camera on a tripod pointing directly at the pit wall, we made video recordings of the tests at 240 frames per second. We stood off to the side during the ECTs while tapping so as not to obstruct the camera view of the markers (Fig. 1).

A challenge encountered during ECTs was that snow often fell in front of the markers directly below the snow shovel during tapping, and markers fell out of the pit wall as the block was compressed (Fig. 1b). This made it difficult, or in some cases impossible, to accurately track the displacement of markers immediately below the shovel. This problem did not affect markers further away from the shovel.

2.2. Data analysis

We utilized a particle tracking velocimetry (PTV) algorithm to analyze the displacement of the markers in the images of the video recording (Crocker and Grier, 1996). Coordinates are assigned to the centroid of each marker by using a spatial band pass filter to search for a local brightness minima. In this way, the position of the markers in each video frame can be determined with a mean accuracy of 0.1 mm. The accuracy of the particle tracking software depends on the size and the quality of the images, i.e. signal-to-noise ratio.

We used a coordinate system aligned with the slope: the x-axis pointing in down-slope direction parallel to the snow surface, the z-axis pointing towards the ground normal to the snow surface. We defined the displacement of a marker in the slope parallel direction u_x and in the slope normal direction u_z as the displacement relative to the initial position, that is, the average position of the marker prior to movement. In the following, absolute displacements $U = \sqrt{u_x^2 + u_z^2}$ are also reported. For propagating cracks, there is a delay between u_z of subsequent markers. The time delay between the onset of movement between markers is proportional to the distance between the markers and was used to calculate the propagation speed c of fracture, as outlined in van Herwijnen and Jamieson (2005). We estimated uncertainties in c using a Monte Carlo method to account for the PTV measurement uncertainty and uncertainties associated with the scaling distance measurement ($\pm 1\%$). By making 10^3 random draws from the probability distributions for the input quantities (assumed normal), we evaluated the resulting distribution. The values of c reported here are the mean of the respective distributions and the reported uncertainty is twice the standard deviation of the respective distributions, which gives a level of confidence of approximately 95%.

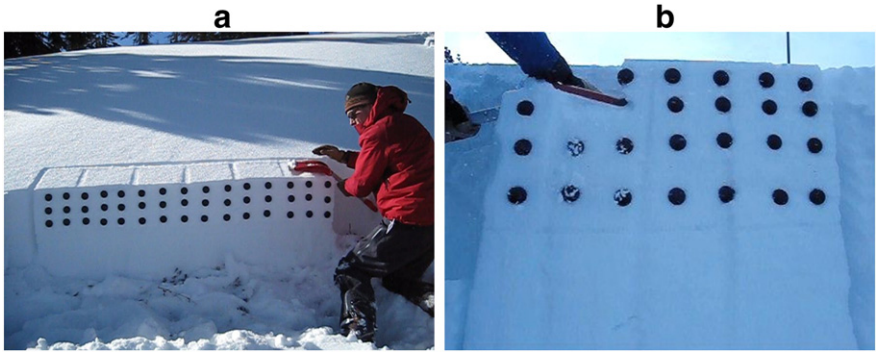

Fig. 1. (a) The experimental setup consisted of recording ECTs with black makers inserted into the pit wall on high speed videos. (b) During tapping, falling snow partially obscured markers directly under the shovel, making tracking those markers difficult or impossible.

3. Results

We analyzed the displacement of the slab in 19 ECTs and 11 PSTs at seven different sites with slope angles (θ) ranging from 10 to 35° (Table 1). The majority of weak layers consisted of buried surface hoar (SH), while one weak layer consisted of depth hoar (DH) and one of faceted grains (FC). We tested a variety of slabs (Fig. 2), including soft new snow (site D), soft faceted snow (sites A, F and G), rounded snow (sites B and E), and wind deposited snow (site C). Slab thickness, measured vertically, ranged from 0.32 to 0.67 m and mean slab density ranged from 143 to 316 kg m^{-3}.

3.1. Snow displacement in ECTs

Tapping on the block during ECTs mainly compacted the snow directly below the snow shovel and had little influence deeper in the snow cover or further away from the shovel. For example, the snow column in test ECT_E1 was substantially compressed directly below the shovel prior to weak layer fracture (Fig. 3a and b). In this experiment, the weak layer consisted of buried surface hoar which fractured after 17 taps. Fracture arrested before crossing the entire column and a crack through the slab occurred approximately halfway through the column (Fig. 3b). The absolute displacement of markers in the upper half of the slab directly below the shovel exhibited the largest displacements (dark and light blue curves in Fig. 3c). On the other hand, prior to weak layer fracture, we did not measure any displacement of markers closer to the weak layer and further away from the shovel (green, orange and red curves in Fig. 2c). Note that for these latter markers the displacements observed after each tap, indicated with the dashed lines in Fig. 3c, were artifacts resulting from snow falling in front of the markers.

Prior to weak layer fracture, we did not measure any displacement of the markers closest to the weak layer in ECTNs, i.e. ECTs in which the fracture arrested before crossing the entire column. In ECT_F2, the initial weak layer fracture was not observed in the field. Subsequent taps then resulted in additional weak layer compaction (Fig. 4a). In all ECTPs, i.e. ECTs in which the fracture crossed the entire column, we also did not observe any displacement for markers closest to the weak layer prior to weak layer fracture. This is clearly seen for a row of markers directly above the weak layer in test ECT_B1 in Fig. 4b. These results also show that slab displacement due to weak layer fracture starts at the free end of the column before propagating to the other side. This behavior was observed in all ECTPs.

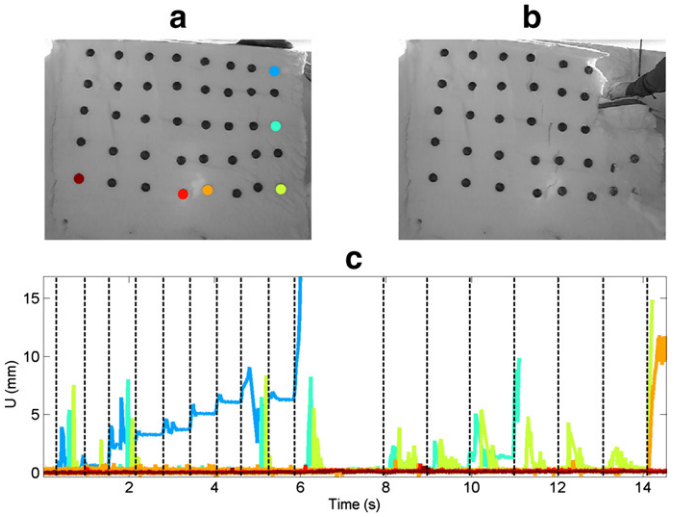

Fig. 3. Results from experiment ECT_E1 (ECTN 17). (a) Image taken at the start of the test. The colored dots show the markers for which the displacements are shown. (b) Image taken at the end of the test showing considerable crushing of the column, partial weak layer fracture and a slab fracture. (c) Total displacement with time. The colors of the displacement curves correspond to the markers indicated with the colored dots in (a). The dashed lines correspond to taps.

In all our ECTs, u_z ranged from 0.04 to 19.4 mm in the area where the weak layer fractured (Table 2). In ECTPs, u_z after weak layer fracture either decreased (ECT_D3, ECT_D4, ECT_D5 and ECT_F1) or increased (ECT_B1 and ECT_B2) throughout the column (Fig. 5a). In ECTNs, on the other hand, u_z decreased to zero typically within 0.30 to 0.60 m from the free edge of the column (Fig. 5b). Note that in some experiments we could not determine the total slope normal displacement due to sliding of the block after weak layer fracture.

3.2. Snow displacement in PSTs

Progressively sawing the weak layer during PSTs resulted in bending of the slab prior to weak layer fracture, as previously reported (Bair et al.,

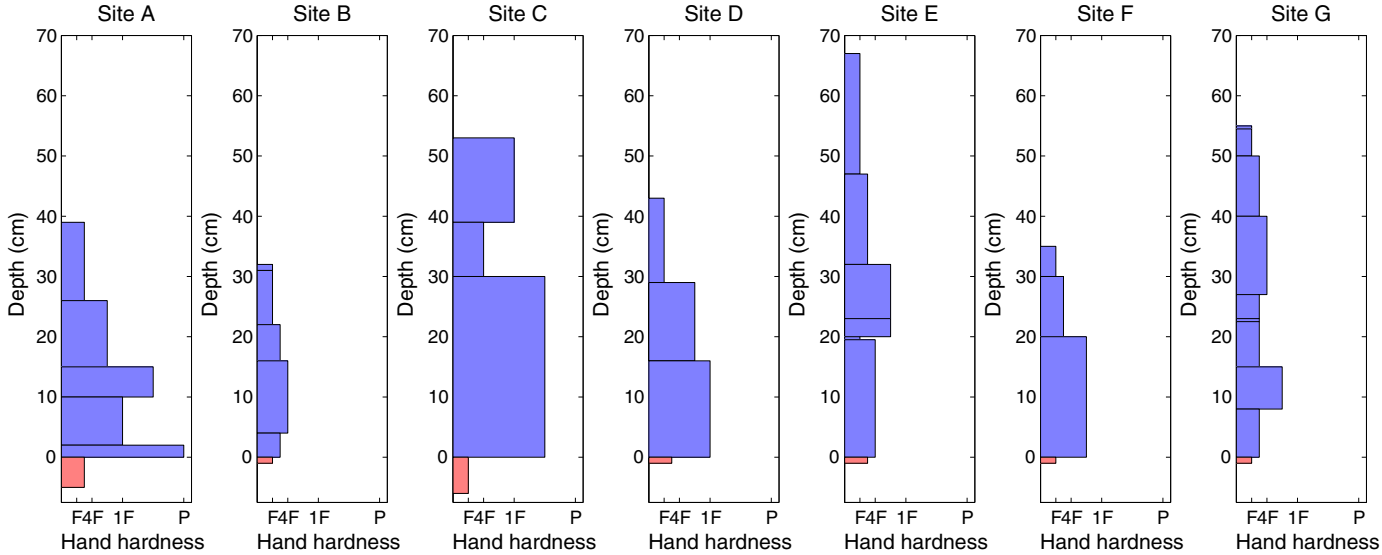

Fig. 2. Overview of the snow stratigraphy at each site. The hand hardness is shown for the layers above the weak layer (blue) as well as for the weak layer (red). The depth is shown relative to the top of the weak layer.

2012; van Herwijnen and Heierli, 2010). While the slope normal displacement associated with slab bending was generally small, on the order of 0.1 mm, it was clearly observed in the u_z curves of markers closest to the free end of the column, independent of subsequent fracture distances (arrows in Fig. 6). Like in ECTs, slab displacement caused by weak layer fracture started at the free end of the column before propagating to the other end of the column (Fig. 6). Note that in experiment PST_F1 the initial weak layer fracture was not observed in the field. Subsequent sawing then resulted in additional and abrupt weak layer collapse (Fig. 6b).

After weak layer fracture, u_z ranged from 0.8 to 11.8 mm in the PSTs (Table 2). In PSTs where the weak layer fractured through the entire column, u_z after weak layer fracture generally decreased (PST_B1, PST_C1, PST_C2 and PST_G1) along the column, except for experiment PST_B2 (Fig. 7a). In PSTs where the weak layer did not fracture through the entire column, u_z decreased to zero within 0.5 to 0.8 m from the free edge of the column (Fig. 7b).

3.3. Propagation speed

Propagation speeds in ECTPs ranged from 8 to 42 m s^{-1} (Table 2), while in PSTs c ranged from 9 to 32 m s^{-1} (Table 3). Despite our relatively short columns, small variations in c with distance were observed (not shown), although no consistent trend was present. Propagation speeds in ECTs either increased (ECT_A4, ECT_A5, ECT_B1, ECT_B2 and ECT_D3), were relatively constant (ECT_C1 and ECT_D5), or decreased (ECT_A1, ECT_D4 and ECT_F1). Likewise, propagation speeds in PSTs either increased (PST_B2), were relatively constant (PST_A2, PST_C1, PST_C2 and, PST_E2), or decreased (PST_B1 and PST_G1).

We measured the propagation speed for both ECTs and PSTs at three sites (sites A, B and C). Values from both tests were in reasonable agreement, except for site C, where c measured in the ECT was larger than in both adjacent PSTs (compare Tables 2 and 3). Despite the large range of c values, they are consistent with previous measurements (Johnson et al., 2004; van Herwijnen and Jamieson, 2005; van Herwijnen et al., 2010) (Fig. 8). Combining our data with data from previous studies results in a statistically significant relationship between propagation speed and mean slab density (Pearson r = 0.5, p = 2.10^{-3}; Fig. 8a). Furthermore, c also correlated significantly with u_z (Pearson r = 0.6,

Table 2
Overview of ECT results and PTV measurements.

Test	Test result	W (m)	ϵ (mm)	u_z (mm)	c (m s^{-1})
ECT_A1	ECTP 12[a]	1.45	0.2	–	20 ± 3
ECT_A2	ECTN 18	1.25	0.3	–	–
ECT_A3	ECTN 11	1.45	0.3	6.5–2.3	–
ECT_A4	ECTP 22[a]	1.3	0.2	–	24 ± 9
ECT_A5	ECTP 16[a]	0.9	0.05	–	17 ± 5
ECT_B1	ECTP 3	1.2	0.06	6.4–3.7	14 ± 2
ECT_B2	ECTP 7	1.9	0.1	6.6–2.1	14 ± 2
ECT_C1	ECTP 17[a]	1.4	0.1	–	42 ± 9
ECT_D1	ECTN 19	1.4	0.1	4.6–1.7	–
ECT_D2	ECTN 20[b]	1.1	0.2	1.5–0.7	–
ECT_D3	ECTP 21	1.0	0.2	9.9–5.1	15 ± 2
ECT_D4	ECTP 25	1.05	0.1	10.6–5.3	20 ± 7
ECT_D5	ECTP 23	1.0	0.2	9.3–4.9	15 ± 3
ECT_E1	ECTN 17[b]	1.35	0.1	19.4–1.2	–
ECT_F1	ECTP 11	1.0	0.06	4.4–0.5	8 ± 6
ECT_F2	ECTN 15[b]	1.05	0.03	1.6–0.04	–
ECT_F3	ECTN 11[b]	1.05	0.03	4.6–0.05	–
ECT_G1	ECTN 16	1.0	0.06	11.6–0.7	–
ECT_G2	ECTN 18	0.95	0.03	3.8–1.7	–

ECT results are shown according to Greene et al. (2010): ECTP## — fracture initiates and propagates across the entire column on tap ##; ECTN## — fracture initiates without full propagation on tap ##. Width of the column (W), PTV measurement accuracy (ϵ), the range of slope normal displacement in the area where the weak layer fractured (u_z) and fracture speed with measurement uncertainty (c) are also shown.

[a] The column slid down-slope after fracture.

[b] Fracture propagation beyond the area below the shovel but not across the entire column.

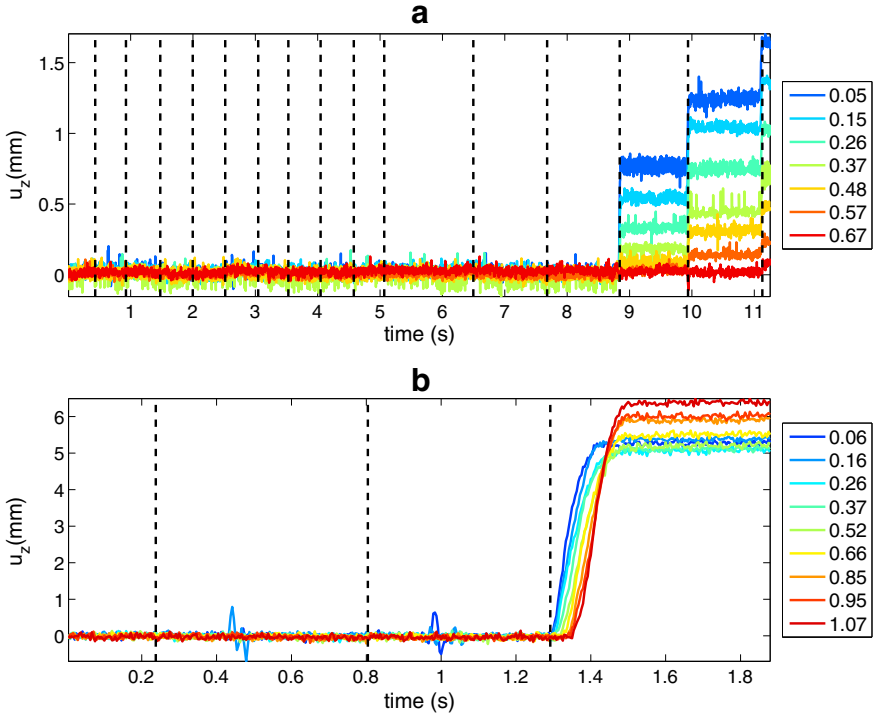

Fig. 4. Slope normal displacement with time for the row of marker closest to the weak layer in tests (a) ECT_F2 (ECTN 15) and (b) ECT_B1 (ECTP 3). The colors of the lines correspond to the distance of the markers to the free edge of the column in m, as indicated in the legend. The dashed lines correspond to taps.

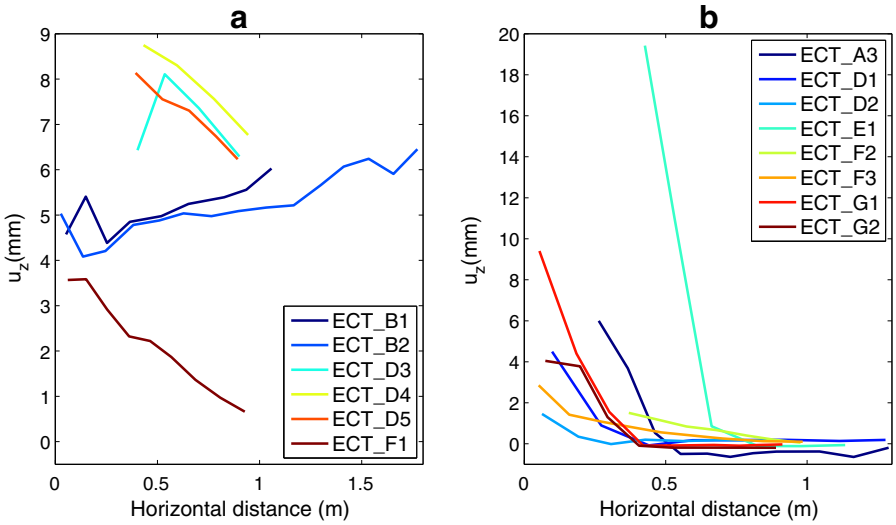

Fig. 5. Mean total slope normal displacement after weak layer fracture with horizontal distance along the column for (a) ECTPs and (b) ECTNs. The colors of the lines correspond to the experiments indicated in the legend.

$p = 5.10^{-4}$; Fig. 8b), confirming results previously reported by van Herwijnen and Jamieson (2005).

4. Discussion

While the PST has been the subject of several detailed studies focusing on fracture initiation, fracture propagation and crack face friction (Bair et al., 2012; van Herwijnen and Heierli, 2009, 2010; van Herwijnen and Jamieson, 2005), thus far the processes leading to weak layer fracture and fracture propagation in the ECT are mostly unknown. The results presented here therefore provide valuable insight into the mechanics of the ECT and allow for a detailed comparison with the PST. Note that in some cases we used non-standard test columns in our experiments. Some caution is therefore warranted when applying our results to standard tests, as very little is known about the influence of test geometry on results.

Overall, the measurements suggest that there is no gradual damage accumulation in the weak layer during tapping in an ECT. Indeed, no noticeable displacement was observed in markers directly above the weak layer prior to fracture (Figs. 3 and 4). Furthermore, the measurements also show that tapping on the column mainly compresses the snow directly below the shovel and does not affect the far end of the column (Fig. 3). We therefore hypothesize that weak layer fracture in an ECT can only occur after the slab has been compressed enough to transmit sufficient stress to the weak layer for fracture. At the critical loading step, the weak layer abruptly fractures over an area roughly equal to the width of the shovel, since in most ECTNs u_z decreased to zero within 0.3 to 0.4 m from the free edge of the column (Fig. 5b). Thus, in our mostly soft slabs, critical crack lengths were roughly 0.3 to 0.4 m. Harder slabs may differ in this respect.

In contrast, in a PST an unstable crack is created by gradually cutting the weak layer with a snow saw until crack propagation begins. Even though critical crack lengths in PSTs are typically around 0.2 to 0.4 m, longer critical crack lengths have also been documented (e.g. Ross and Jamieson, 2012). Progressively cutting the weak layer with a snow saw results in bending of the overlying snow slab (Fig. 6), providing the energy necessary for crack propagation (Bair et al., 2012; Heierli et al., 2008; Sigrist and Schweizer, 2007; van Herwijnen and Heierli, 2010). Thus, when performing a PST, slab properties are not altered as they are during an ECT.

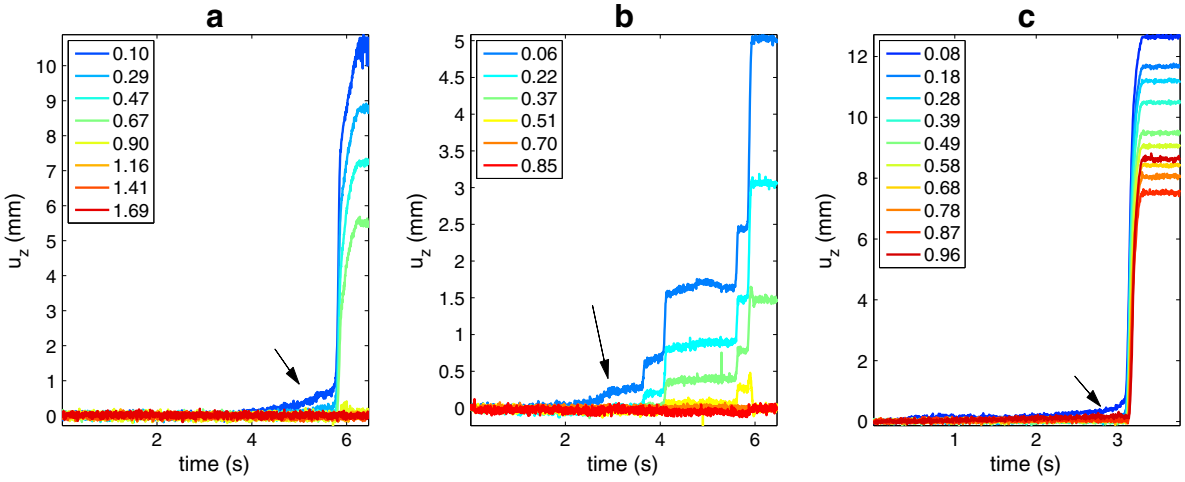

Fig. 6. Slope normal displacement with time for the row of markers closest to the weak layer in tests (a) PST_D1, (b) PST_F1 and (c) PST_B1. The colors of the lines correspond to the distance of the markers to the free edge of the column in m, as indicated in the legend. The arrows indicate the marker displacement associated with slab bending prior to weak layer fracture.

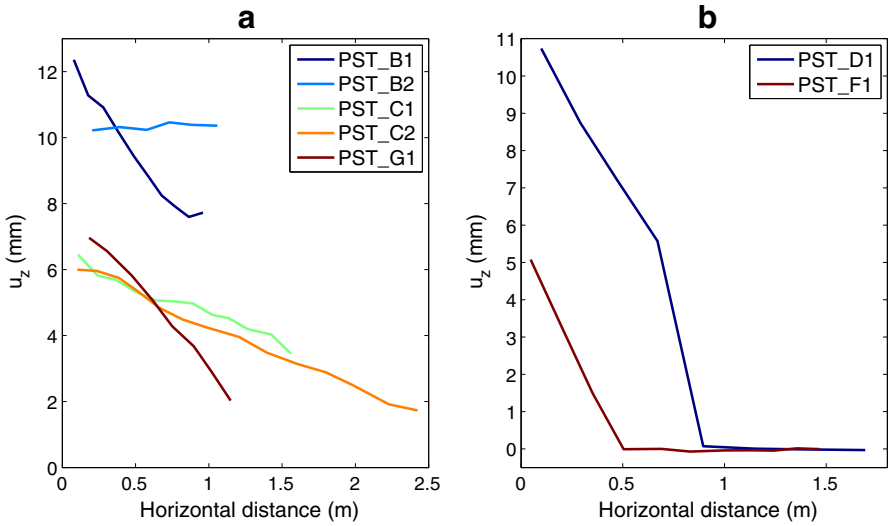

Fig. 7. Mean total slope normal displacement after weak layer fracture with horizontal distance along the column for (a) PSTs with complete weak layer fracture and (b) PSTs with partial weak layer fracture. The colors of the lines correspond to the experiments indicated in the legend.

Though the processes involved in reaching the critical crack length prior to propagation differ for ECTs and PSTs, our observations on weak layer fracture are consistent for both tests. First, the total slope normal displacement after weak layer fracture was similar (compare Figs. 5 and 7). This result also confirms that tapping on the snow column in ECTs does not result in increased weak layer collapse, as already observed for compression tests by van Herwijnen and Jamieson (2005). Second, similar fluctuations were observed in the total slope normal displacement after weak layer collapse in both tests. These likely relate to small scale changes in microstructural properties of the weak layer (e.g. crystal size or layer thickness) and have also been observed in much longer PSTs (van Herwijnen et al., 2010). Third, in both tests, slab displacement due to weak layer fracture starts at the free end of the column and propagates to the other end (compare Figs. 4b and 6c). Fourth, if crack propagation arrests before crossing the entire column, subsequent tapping or sawing results in further compaction of the weak layer (compare Figs. 4a and 6b). Fifth, observed crack propagation speeds were similar for both tests (Fig. 8), and no consistent trends in c were observed. This is in line with results presented by van Herwijnen et al. (2010), who found no consistent trend in propagation speeds in much longer PSTs. All in all, our observations on crack propagation in ECTs are consistent with results obtained from PSTs.

Table 3
Overview of PST results and PTV measurements.

Test	r_c (m)	L (m)	ϵ (mm)	u_z (mm)	c (m s^{-1})
PST_A1	0.27[a, b]	1.35	0.2	–	–
PST_A2	0.26[a]	1.35	0.3	–	17 ± 1
PST_B1	0.17	1.2	0.3	12.7–6.4	17 ± 2
PST_B2	0.15	1.3	0.2	1.0–1.1	21 ± 4
PST_C1	0.38	1.7	0.1	7.3–3.5	27 ± 4
PST_C2	0.44	2.55	0.1	6.2–1.4	24 ± 3
PST_D1	0.34[b]	2.05	0.1	11.8–4.8	–
PST_E1	0.32[a, b]	1.15	0.1	–	–
PST_E2	0.07[a]	1.0	0.05	–	32 ± 8
PST_F1	0.22[b]	1.55	0.06	5.3–0.8	–
PST_G1	0.32	1.4	0.06	7.1–2.0	16 ± 3

Critical cut length (r_c), column length (L), PTV measurement accuracy (ϵ), the range of slope normal displacement in the area where the weak layer fractured (u_z) and fracture speed with measurement uncertainty (c) are shown.
[a] The column slid down-slope after fracture.
[b] Weak layer fracture arrested before reaching the end of the column.

From a practical point of view, our measurements show that ECT and PST results relate to fracture initiation and propagation, both of which are necessary for avalanche release. Both these snow stability tests therefore provide valuable information with regard to snow slope stability evaluation, as already shown in various studies (e.g. Ross and Jamieson, 2012; Simenhois and Birkeland, 2009; Winkler and Schweizer, 2009). However, many questions remain as to how results from small scale stability tests relate to large scale processes involved in avalanche release, such as the influence of the free edges on test results, the significance of partial crack propagation and the role of snow slab compaction in ECTs.

5. Conclusions

Using high-speed video recordings in combination with particle tracking velocimetry, we analyzed the displacement of the snow slab in 19 ECTs and 11 PSTs at seven different sites. Despite the fact that the ECT is a widely used snowpack stability test, little was known about what happens to the slab and weak layer during the test. Our results partially fill this gap, providing a better understanding of the mechanics of the ECT. Our results lead to some important conclusions:

1. Tapping only affects the snow immediately below the shovel since we did not observe any marker displacement at the far end of the column prior to weak layer fracture. This suggests that the ECT is indexing not only crack initiation, but also crack propagation.
2. Tapping mainly compresses the slab. We did not observe any progressive damage in the weak layer prior to fracture, when the weak layer collapses.
3. Propagation speeds measured in ECTs were consistent with measurements in adjacent PSTs and previously published results.

During fracture, weak layers in ECTs compact on the order of several mm, similar to measurements obtained from PSTs. Measured propagation speeds (on the order of 20 to 30 ms^{-1}) are also similar to those from PSTs. The similarities between our results and those with PSTs give us confidence that the fracture mechanics are similar regardless of the triggering mechanism.

However, important differences do exist between the PST and ECT. In a PST, an unstable crack is created by cutting the weak layer with a snow saw until crack propagation occurs. The crack length is thus gradually increased resulting in bending of the overlying slab. On the other hand, with the ECT the fracture is initiated by tapping on the top of

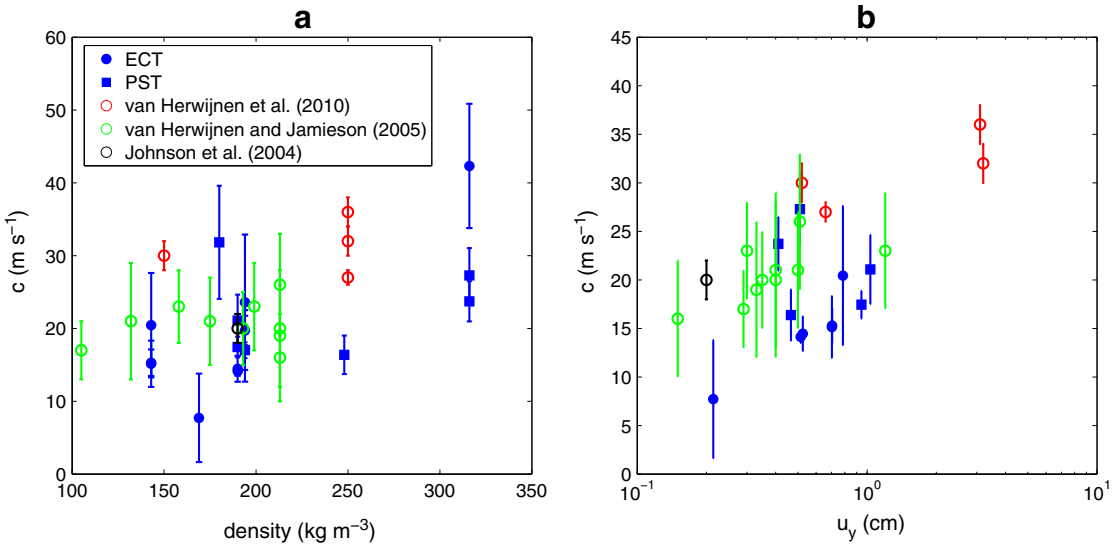

Fig. 8. (a) Propagation speed with mean slab density. (b) Propagation speed with mean total slope normal displacement after weak layer fracture. Note the logarithmic scale. The bars indicate the measurement uncertainty.

the block. No sign of progressive damage in the weak layer was observed, and it appears that at the critical loading step, i.e. the final tap, the weak layer fractures over an area directly under the shovel. Depending on snow conditions, this crack will either be large enough to propagate or fracture will arrest.

Building on observational studies which show that ECT results correlate with stability (e.g. Simenhois and Birkeland, 2009), this study shows that ECT results relate to fracture initiation and propagation, both of which are required for avalanche release. Though this increases our confidence in ECT results for assessing avalanche danger, we continue to caution people that stability tests are only one part of avalanche danger assessments. In the end, a holistic approach utilizing weather, snowpack, and avalanche observations, in addition to stability test results, is necessary for good decision-making in avalanche terrain.

Acknowledgments

We thank Ron Simenhois for reviewing this paper for us. Thanks also go to the Gallatin National Forest Avalanche Center for providing information and logistical support for this work, and to Brad Carpenter, Wes Farnsworth, Eric Knoff, Alex Marienthal, and Robyn Wooldridge for helping out in the field.

References

Bair, E., Simenhois, R., Birkeland, K., Dozier, J., 2012. A field study on failure of storm snow slab avalanches. Cold Regions Science and Technology 79–80, 20–28.
Birkeland, K.W., Chabot, D., 2012. Changes in stability test usage by SnowPilot users. Proc. 2012 Int. Snow Sci. W., Anchorage, AK, USA, pp. 1065–1068.
Chabot, D., Kahrl, M., Birkeland, K., Anker, C., 2004. SnowPilot: a "new school" tool for collecting, graphing, and databasing snowpit and avalanche occurrence data with a PDA. Proc. 2004 Int. Snow Sci. W., Jackson Hole, WY, USA, p. 476.
Crocker, J., Grier, D., 1996. Methods of digital video microscopy for colloidal studies. Journal of Colloid and Interface Science 179, 298–310.
Föhn, P., 1987. The "Rutschblock" as a practical tool for slope stability evaluation. IAHS-AISH Publ. 162, pp. 223–228.
Gauthier, D., Jamieson, B., 2006. Evaluating a prototype field test for weak layer fracture and failure propagation. Proc. 2006 Int. Snow Sci. W., Telluride, CO, USA, pp. 107–116.
Gauthier, D., Jamieson, B., 2008. Evaluation of a prototype field test for fracture and failure propagation propensity in weak snowpack layers. Cold Regions Science and Technology 51, 87–97.
Greene, E., Atkins, D., Birkeland, K., Elder, K., Landry, C., Lazar, B., McCammon, I., Moore, M., Sharaf, D., Sterbenz, C., Tremper, B., Williams, K., 2010. Snow, Weather and Avalanches: Observation Guidelines for Avalanche Programs in the United States. American Avalanche Association, Pagosa Springs, CO, USA.
Heierli, J., 2008. Anticrack Model for Slab Avalanche Release. Ph.D. thesis Universität Karlsruhe (TH).
Heierli, J., Gumbsch, P., Zaiser, M., 2008. Anticrack nucleation as triggering mechanism for slab avalanches. Science 321, 240–243.
Jamieson, J., 1999. The compression test after 25 years. The Avalanche Review 18, 10–12.
Johnson, B.C., Jamieson, J.B., Stewart, R.R., 2004. Seismic measurements of fracture speed in a weak snowpack layer. Cold Regions Science and Technology 40, 41–45.
Ross, C., Jamieson, B., 2008. Comparing fracture propagation tests and relating test results to snowpack characteristics. Proc. 2008 Int. Snow Sci. W., Whistler, BC, Canada, pp. 376–385.
Ross, C., Jamieson, B., 2012. The Propagation Saw Test: slope scale validation and alternative test methods. Journal of Glaciology 58, 407–416.
Schweizer, J., Jamieson, B., 2010. Snowpack tests for assessing snow-slope stability. Annals of Glaciology 51, 187–193.
Schweizer, J., Jamieson, J., Schneebeli, M., 2003. Snow avalanche formation. Reviews of Geophysics 41, 1016.
Sigrist, C., Schweizer, J., 2007. Critical energy release rates of weak snowpack layers determined in field experiments. Geophysical Research Letters 34, L03502.
Simenhois, R., Birkeland, K., 2006. A field test for fracture initiation and propagation. Proc. 2006 Int. Snow Sci. W. Workshop, Telluride, CO, USA, pp. 79–85.
Simenhois, R., Birkeland, K.W., 2009. The Extended Column Test: test effectiveness, spatial variability, and comparison with the Propagation Saw Test. Cold Regions Science and Technology 59, 210–216.
van Herwijnen, A., Heierli, J., 2009. Measurement of crack-face friction in collapsed weak snow layers. Geophysical Research Letters 36, L23502.
van Herwijnen, A., Heierli, J., 2010. A field method for measuring slab stiffness and weak layer fracture energy. Proc. 2010 Int. Snow Sci. W., Lake Tahoe, CA, USA, pp. 232–237.
van Herwijnen, A., Jamieson, B., 2005. High-speed photography of fractures in weak snowpack layers. Cold Regions Science and Technology 43, 71–82.
van Herwijnen, A., Jamieson, B., 2007a. Fracture character in compression tests. Cold Regions Science and Technology 47, 60–68.
van Herwijnen, A., Jamieson, B., 2007b. Snowpack properties associated with fracture initiation and propagation resulting in skier-triggered dry snow slab avalanches. Cold Regions Science and Technology 50, 13–22.
van Herwijnen, A., Schweizer, J., Heierli, J., 2010. Measurement of the deformation field associated with fracture propagation in weak snowpack layers. Journal of Geophysical Research – Earth 115, F03042.
Winkler, K., Schweizer, J., 2009. Comparison of snow stability tests: extended column test, Rutschblock test and compression test. Cold Regions Science and Technology 59, 217–226.